Materials Research. 2018; 21(2): e20160533
DOI: http://dx.doi.org/10.1590/1980-5373-MR-2016-0533

Preparation and Characterization of Nickel ferrite Nanoparticles via Co-precipitation Method

Suresh Sagadevan[a]**, Zaira Zaman Chowdhury[b], Rahman F. Rafique[c]

[a]Centre for Nanotechnology, AMET University, Chennai-603 112, India
[b]Nanotechnology & Catalysis Research Centre, University of Malaya, Kula Lumpur 50603, Malaysia
[c]Department of Environmental Sciences, Rutgers University, New Brunswick, NJ 08901-8551, USA

Received: July 14, 2016; Revised: December 06, 2017; Accepted: December 18, 2017

Nickel ferrite ($NiFe_2O_4$) nanoparticles were synthesized using co-precipitation method. The X-ray diffraction (XRD) pattern was used to determine the structure of $NiFe_2O_4$ nanoparticles. The presence of $NiFe_2O_4$ nanoparticles was confirmed by the FT-IR spectrum. The details of the surface morphology of $NiFe_2O_4$ nanoparticles were obtained by Scanning Electron Microscopic analysis. The particle size of the $NiFe_2O_4$ nanoparticles could be determined by means of Transmission Electron Microscopy. This work aimed at the investigation of the dielectric properties such as the dielectric loss and the dielectric constant of $NiFe_2O_4$ nanoparticles at varied frequencies and temperatures. In addition, the magnetic properties of the $NiFe_2O_4$ nanoparticles were studied.

Keywords: *Nickel ferrite ($NiFe_2O_4$), XRD, FT-IR, SEM, TEM and Magnetic properties.*

1. Introduction

The last few decades saw substantial development in the field of nano technology, particularly in physical sciences. The synthesis of nano crystalline spinel ferrites plays an important role in determining their physical properties at nano and sub nano levels. Ferrites have established their potential in several applications due to their remarkable electrical and magnetic properties, and also in magnetic resonance imaging (MRI) enhancement, magnetic high-density information storage etc. Nickel ferrite is one of the multifaceted and technologically important soft ferrite materials because of its typical ferrimagnetic properties, lower eddy current losses, low conductivity and high electrochemical stability[1,2]. Nickel ferrite ($NiFe_2O4$) has a counter spinel structure. The location of the divalent cations (Ni^{2+}) in the crystal structure is almost homologous to the magnetic properties of the nickel ferrite. However, nickel ferrite shows super-paramagnetic nature and it has diverse applications such as gas-sensor, magnetic fluids, catalysts, magnetic storage systems, photomagnetic materials, site-specific drug delivery, magnetic resonance imaging and microwave devices[3-7]. Various methods such as hydrothermal method[8], co-precipitation method[9], gel-assistant hydrothermal route[10], thermolysis[11], wet chemical co-precipitation technique[12], self-propagating[13], have been developed to prepare nanocrystallite nickel ferrite. This paper focuses on the synthesis of $NiFe_2O_4$ nanoparticles using the co-precipitation method, their characterization by means of powder X-ray diffraction, Scanning Electron Microscopy (SEM), FTIR, Transmission Electron Microscope (TEM), and the determination of the dielectric properties and the magnetic behaviour of $NiFe_2O_4$ nanoparticles.

*e-mail: sureshsagadevan@gmail.com

2. Experimental procedure

Nickel ferrite ($NiFe_2O_4$) nanoparticles were synthesized via co-precipitation method. Typical synthetic procedures required analytical grade 3M solution of sodium hydroxide (NaOH) which was slowly added to salt solutions of 0.4M ferric chloride ($FeCl_3$) and 0.2 M nickel chloride ($NiCl_2$). The pH of the solution was constantly observed as the NaOH solution was added drop wise. The reactants were consistently stirred using a magnetic stirrer until a pH level of >12 was achieved. A specified amount of oleic acid was added to the solution as the surfactant. The liquid precipitate was then brought to a reaction temperature of 80°C and stirred for 30 min. The product was cooled to room temperature and then washed twice with distilled water and ethanol to eliminate unwanted impurities and the residual surfactant from the prepared sample. Finally, the sample was centrifuged and then dried overnight at about 80°C. The acquired substance was then ground into a fine powder.

3. Results and Discussion

3.1 XRD analysis

The XRD pattern of the $NiFe_2O_4$ nanoparticles was recorded by using a powder X-ray diffractometer {Schimadzu model: XRD 6000 using CuKα (λ=0.154 nm) radiation}, with a diffraction angle between 30º and 60º. Figure 1 shows the XRD patterns of the as-prepared $NiFe_2O_4$ nanoparticles.

The patterns show the formation of single phase cubic spinal crystal structure. The $NiFe_2O_4$ nanoparticles contained no impurity peaks within the limit of X-ray detection. The broad peaks of X-ray diffraction patterns stipulate that the particles of the synthesized samples are in nanometer range. The average crystallite size of the samples could be calculated using Scherrer's formula

$$D = \frac{0.9\lambda}{\beta \cos\theta} \quad (1)$$

where λ is the X-ray wavelength (CuK_α radiation and equals to 0.154 nm), θ is the Bragg diffraction angle, and β is the FWHM of the XRD peak appearing at the diffraction angle θ. The average crystalline size was calculated from the X-ray line broadening using Scherrer equation and it was found to be about 18 nm which is almost similar to the reported value 16 nm[14].

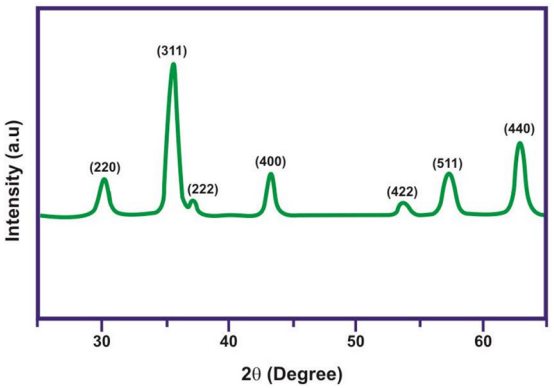

Figure 1. XRD pattern of $NiFe_2O_4$ nanoparticles.

3.2 FTIR analysis

The FTIR spectrum of the $NiFe_2O_4$ nanoparticles was taken using an FTIR model Bruker IFS 66W Spectrometer. In order to determine the chemical structure of the sample, the FTIR spectrum was observed above the frequency range of 4000-500 cm^{-1} as shown in Figure 2. The decomposition of hydroxide to oxide phase for the formation of spinel ferrites was well reflected in the FTIR spectrum. It has been reported that the IR bands of solids are usually attributed to the vibration of ions in the crystal lattice. The bands at 552 cm^{-1} and 464 cm^{-1} represented tetrahedral and octahedral modes of $NiFe_2O_4$, respectively[15]. The band located at 3389 cm^{-1} could be attributed to the symmetric vibration of -OH groups. The bands with peaks observed at 1038 cm^{-1} could be assigned to O-H bending vibration[16]. The peak at 2333 cm^{-1} was ascribed to H-O-H bending vibration of the free or absorbed water[17].

3.3 SEM analysis

SEM studies were carried out using JEOL, JSM- 67001. The samples needed a coating of gold for SEM analysis for the avoidance of charging effect. The morphology and the size distribution of the $NiFe_2O_4$ nanoparticles were determined using SEM. Typical SEM images of $NiFe_2O_4$ synthesized particles are shown in Figure 3. SEM micrograph depicts that the samples contain micrometrical aggregation of tiny particles. The existence of high dense agglomeration indicates that pore free crystallites are present on the surface. The SEM images show the agglomerated form of $NiFe_2O_4$ nanoparticles. As the nanoparticles possess high surface energies, they tend to agglomerate and grow into larger assemblies.

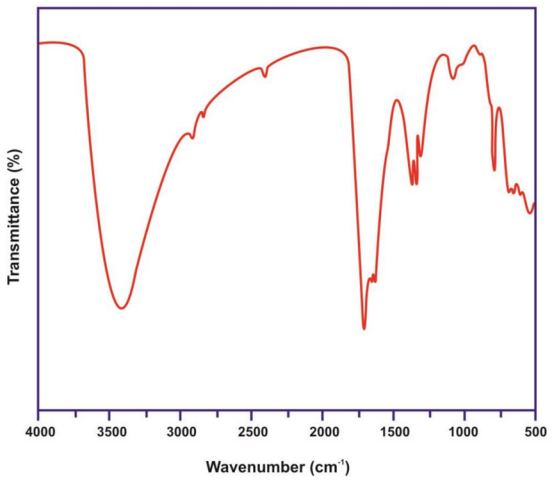

Figure 2. FTIR spectrum of $NiFe_2O_4$ nanoparticles.

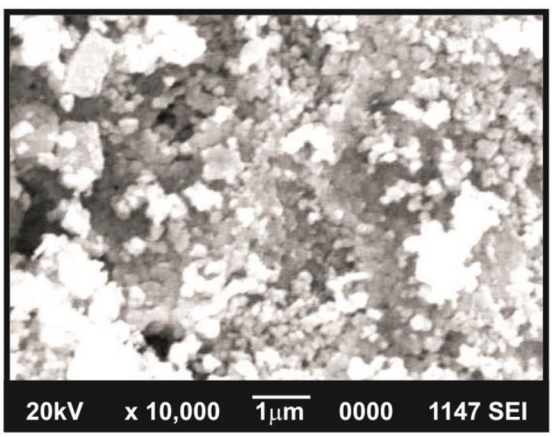

Figure 3. SEM image of $NiFe_2O_4$ nanoparticles.

3.4 TEM analysis

Transmission Electron Microscopic (TEM) image was taken using an H-800 Transmission Electron Microscopy (Hitachi, Japan) with an accelerating voltage of 100kV. The colloidal nanoparticles solution had to be dried on the copper grid before analysis. Figure 4 shows the TEM image of the $NiFe_2O_4$ nanoparticles. In the TEM image most of the particles appear to be spherical; however, some elongated particles are also present in the image. Some moderately agglomerated particles as well as segregated particles are also present in the sample. The estimated average size of the nanoparticles by TEM was about 28 nm which was almost similar to that of the reported values[18].

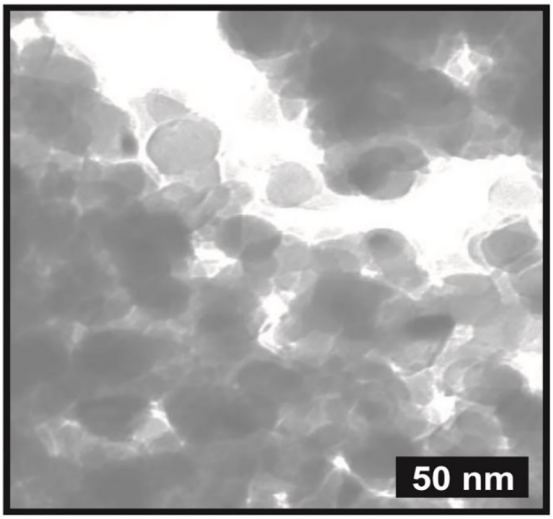

Figure 4. TEM image of $NiFe_2O_4$ nanoparticles.

3.5 Magnetic measurements

The magnetic behavior of $NiFe_2O_4$ nanoparticles was investigated using VSM (Lakeshore VSM 7410). The high coercivity values account for the slower rate of growth of crystallite size that takes place during the heating process. It is not only the temperature but also the morphology that seems to significantly influence the magnetic properties. The increased value of the coercivity could be attributed to the magnetic spin orientation along the axis that eases magnetization[19]. On account of the grain boundaries and free surface, the magnetic properties improved[20]. Figure 5 shows the magnetic hysteresis loops of the $NiFe_2O_4$ nanoparticles at room temperature. The magnetic parameters, namely retentivity, coercivity, and saturation magnetization of the sample were measured to be 3875 G, 0.142emu/g, and 0.343emu/g respectively.

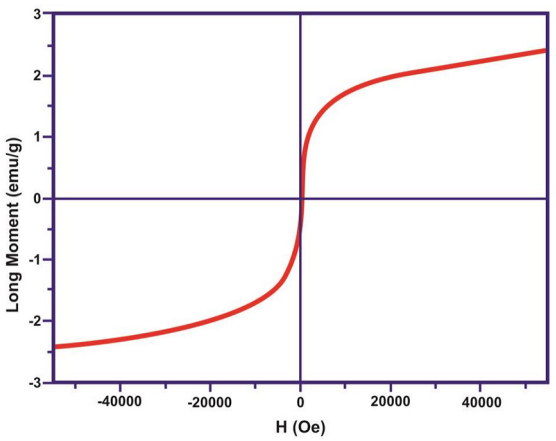

Figure 5. Magnetic properties of $NiFe_2O_4$ nanoparticles.

3.6 Dielectric Properties

The dielectric properties of the $NiFe_2O_4$ nanoparticles were analyzed using an HIOKI 3532-50 LCR HITESTER over the frequency range 50Hz-5MHz. The $NiFe_2O_4$ nanoparticles pellets in disk form were studied at different temperatures. For measurements, the samples were obtained with the diameter of ~10 mm and thickness ~1 mm and a sample was placed between the electrodes having a conventional four terminal sample holder for investigations involving temperature variations along with a conventional two terminal sample holder for ambient conditions alone. The sample was mounted between copper platforms and electrodes. To ensure good electrical contact, the faces were coated with silver paint. The capacitance and the dissipation factor of the parallel plate capacitor which was formed by the copper plate and the electrode having the sample as a dielectric medium were measured. Analysis on the dielectric behaviour of $NiFe_2O_4$ nanoparticles provided much useful information about the electric field distribution within the as grown $NiFe_2O_4$ nanoparticles. At various temperatures and at a frequency ranging from 50Hz to 5MHz the measurements were performed. The dielectric constant and dielectric loss were determined from the equations 2 and 3 respectively.

$$C = \varepsilon_r \varepsilon_0 A/d \tag{2}$$

$$\tan\delta = 1/2 \times 3.14 \times f \times R_P C_P \tag{3}$$

where A is the area of the sample and d is the thickness of the sample. The relative permittivity (ε_r) is usually known as dielectric constant. A study of the dielectric nature of $NiFe_2O_4$ nanoparticles could furnish useful information about the electric field allocation within the $NiFe_2O_4$ nanoparticles. The frequency dependence of the dielectric constant and the dielectric loss at various temperatures is shown in Figures 6 and 7 respectively. It could be learned that both the dielectric constant and the dielectric loss exhibited homologous nature. The dielectric constant of materials is influenced by the totality of electronic, ionic, bipolar and space charge polarizations of the frequencies[21]. All the four polarization mechanisms seem to be active at low frequencies. Lower frequencies and high temperatures normally aid the progress of space charge polarization. The low value of the dielectric constant with increasing frequency could be ascribed to the loose or weak bond of ions at the lower frequency range[22]. Still greater values of the dielectric constant at lower frequency values are possible due to the charge accumulation at the grain boundaries. Another possibility to gain higher values is due to heterogeneous dielectric structure which possesses the interfacial/space charge polarization. Due to the fact that beyond a certain frequency of the external field, the polarization decreased with the increase in frequency and then reached a constant value, the hopping between various metal ions could not follow the alternating field. It was noticed that the value of the dielectric constant decreased with increase in the frequency[23].The dielectric loss is a broad indication of the energy dissipation in the dielectric system.

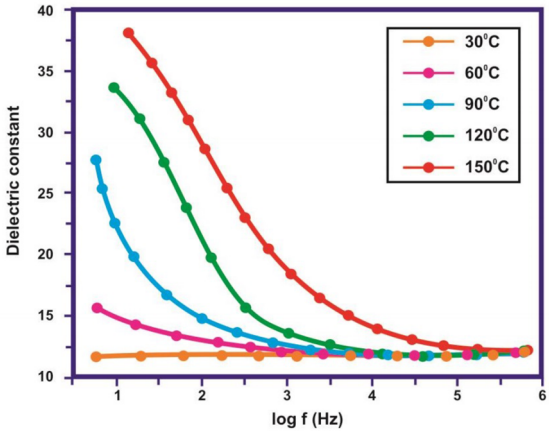

Figure 6. Dielectric constant plot for $NiFe_2O_4$ nanoparticles

Figure 7 shows the curve explaining how the dielectric loss factor varies with the frequency at various temperatures. It becomes clear from the graph that the dielectric loss decreases with the increase in frequency and attains a low value in the high frequency region. The study clearly showed that the dielectric loss suddenly dropped at lower frequencies and attained constancy at higher frequencies. Further, it could be observed that owing to the space charge polarization the dielectric loss decreased with the increase in the frequency for all temperatures[24,25].

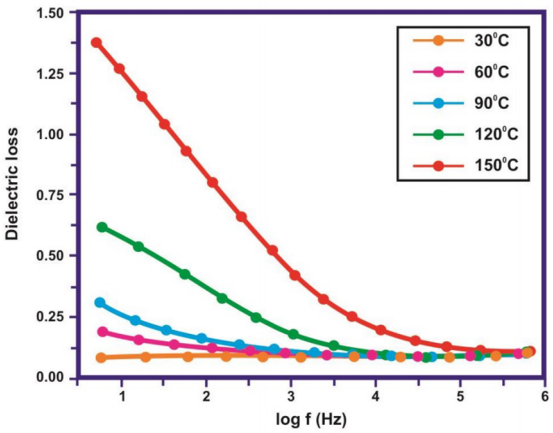

Figure 7. Dielectric loss plot for $NiFe_2O_4$ nanoparticles

4. Conclusion

The paper thoroughly discussed the synthesis of $NiFe_2O_4$ nanoparticles by the employment of co-precipitation method. The fact that the $NiFe_2O_4$ nanoparticles belonged to the cubic spinal structure was established by XRD. FTIR spectrum also supported the formation of $NiFe_2O_4$ nanoparticles. That the nanoparticles agglomerated to form spherical-shaped particles was also confirmed and made clear by the SEM analysis. The average particle size of $NiFe_2O_4$ nanoparticles was found to be 28 nm. The impact of the frequency and the temperature on the dielectric loss and the dielectric constant for $NiFe_2O_4$ nanoparticles was studied. From the dielectric studies it became evident that the frequency negatively impacted both the dielectric constant and the dielectric loss as decreased with increase in the frequency. A study of the magnetic properties was also carried out using VSM measurements.

5. Acknowledgements

This research work has been conducted using UMRG-2017 project under AET Cluster of University Malaya, Malaysia under the Project Principal Investigator Dr. Zaira Zaman Chowdhury from University of Malaya, Malaysia and Co-Investigator Dr. Suresh Sagadevan from AMET University, India. The one of the author Dr.Suresh Sagadevan is grateful to University of Malaya, Malaysia providing financial support to undertake this work.

6. References

1. Zhao G, Xu JJ, Chen HY. Fabrication, characterization of Fe_3O_4 multilayer film and its application in promoting direct electron transfer of hemoglobin. *Electrochemistry Communications*. 2006;8(1):148-154.

2. Zhang T, Tian B, Kong J, Yang P, Liu B. A sensitive mediator-free tyrosinase biosensor based on an inorganic-organic hybrid titania sol-gel matrix. *Analytica Chimica Acta*. 2003;489(2):199-206.

3. Chu X, Jiang D, Zheng C. The preparation and gas-sensing properties of $NiFe_2O_4$ nanocubes and nanorods. *Sensors and Actuators B: Chemical*. 2007;123(2):793-797.

4. Rana S, Srivastava RS, Sorensson MM, Misra RDK. Synthesis and characterization of nanoparticles with magnetic core and photocatalytic shell: Anatase TiO_2-$NiFe_2O_4$ system. *Materials Science and Engineering: B*. 2005;119(2):144-151.

5. Raikher YL, Stepanov VI, Depeyrot J, Sousa MH, Tourinho FA, Hasmonay E, et al. Dynamic optical probing of the magnetic anisotropy of nickel-ferrite nanoparticles. *Journal of Applied Physics*. 2004;96(9):5226-5233.

6. Cunningham CH, Arai T, Yang PC, McConnell MV, Pauly JM, Conolly SM. Positive contrast magnetic resonance imaging of cells labeled with magnetic nanoparticles. *Magnetic Resonance in Medicine*. 2005;53(5):999-1005.

7. Yoon TJ, Kim JS, Kim BG, Yu KN, Cho MH, Lee JK. Multifunctional nanoparticles possessing a "magnetic motor effect" for drug or gene delivery. *Angewandte Chemie (International ed)*. 2005;44(7):1068-1071.

8. Li H, Wu H, Xiao G. Effects of synthetic conditions on particle size and magnetic properties of $NiFe_2O_4$. *Powder Technology*. 2010;198(1):157-166.

9. Sivakumar P, Ramesh R, Ramanand A, Ponnusamy S, Muthamizhchelvan C. Preparation of sheet like polycrystalline $NiFe_2O_4$ nanostructure with PVA matrices and their properties. *Materials Letters*. 2011;65(9):1438-1440.

10. Chen L, Dai H, Shen Y, Bai J. Size-controlled synthesis and magnetic properties of $NiFe_2O_4$ hollow nanospheres via a gel-assistant hydrothermal route. *Journal of Alloys and Compounds*. 2010;91(1-2):L33-L38.

11. Bao N, Shen L, Wang Y, Padhan P, Gupta A. Facile Thermolysis Route to Monodisperse Ferrite Nanocrystals. *Journal of the American Chemical Society*. 2007;129(41):12374-12375.

12. Patange SM, Shirsath SE, Jadhav SS, Lohar KS, Mane DR, Jadhav KM. Rietveld refinement and switching properties of Cr^{3+} substituted $NiFe_2O_4$ ferrites. *Materials Letters*. 2010;64(6):722-724.

13. Cross WB, Affleck L, Kuznetsov MV, Parkin IP, Pankhurst QA. Self-propagating high-temperature synthesis of ferrites MFe_2O_4 (M = Mg, Ba, Co, Ni, Cu, Zn); reactions in an external magnetic field. *Journal of Materials Chemistry*. 1999;9(10):2545-2552.

14. Sivagurunathan P, Gibin SR. Preparation and characterization of nickel ferrite nano particles by co-precipitation method with citrate as chelating agent. *Journal of Materials Science: Materials in Electronics*. 2016;27(3):2601-2607.

15. Guo L, Shen X, Meng X, Feng Y. Effect of Sm^{3+} ions doping on structure and magnetic properties of nanocrystalline $NiFe_2O_4$ fibers. *Journal of Alloys and Compounds*. 2010;490(1-2):301-306.

16. Deb P, Basumallick A, Das S. Controlled synthesis of monodispersed superparamagnetic nickel ferrite nanoparticles. *Solid State Communications*. 2007;142(12):702-705.

17. Ahmed MA, Mansour SF, El-Dek SI. Investigation of the physico-chemical properties of nanometric NiLa ferrite/PST matrix. *Solid State Ionics*. 2010;181(25-26):1149-1555.

18. Aliahmad M, Noori M, Hatefi Kargan N, Sargazi M. Synthesis of nickel ferrite nanoparticles by co-precipitation chemical method. *International Journal of Physical Sciences*. 2013;8(18):854-858.

19. Zhang X, Niu Y, Li Y, Hou X, Wang Y, Bai R, et al. Synthesis, optical and magnetic properties of α-Fe_2O_3 nanoparticles with various shapes. *Materials Letters*. 2013;99(2013):111-114.

20. Straumal BB, Mazilkin AA, Protasova SG, Myatiev AA, Straumal PB, Goering E, et al. Amorphous grain boundary layers in the ferromagnetic nanograined ZnO films. *Thin Solid Films*. 2011;520(4):1192-1194.

21. Sagadevan S, Arunseshan C. Dielectric Properties of Cadmium Selenide (CdSe) Nanoparticles synthesized by solvothermal method. *Applied Nanoscience*. 2014;4(2):179-184.

22. Sagadevan S. Studies on the dielectric properties of CdS nanoparticles. *Applied Nanoscience*. 2014;4(3)325-329.

23. Sagadevan S. Synthesis and Electrical Properties of TiO_2 Nanoparticles Using a Wet Chemical Technique. *American Journal of Nanoscience and Nanotechnology*. 2013;1(1):27-30.

24. Sagadevan S. Synthesis, structural and dielectric properties of zinc sulfide nanoparticles. *International journal of Physical Sciences*. 2013;8(21):1121-1127.

25. Sagadevan S. Study of Structural, Surface Morphological and Dielectric Properties of Cu-doped Tin Oxide Nanoparticles. *Journal of Nano Research*. 2015;34:91-97.